2024 IEEE 25th International Workshop on Signal Processing Advances in Wireless Communications (SPAWC) | 979-8-3503-9318-7/24/$31.00 ©2024 IEEE | DOI: 10.1109/SPAWC60668.2024.10694312

Antenna Position Optimization of Sparse Arrays for Near-Field Multiuser Communications

Kangjian Chen *, Chenhao Qi *, Geoffrey Ye Li †, and Octavia A. Dobre ‡
*School of Information Science and Engineering, Southeast University, Nanjing, China
†Department of Electrical and Electronic Engineering, Imperial College London, London, UK
‡Faculty of Engineering and Applied Science, Memorial University, Canada
Email: kjchen@seu.edu.cn, qch@seu.edu.cn, geoffrey.li@imperial.ac.uk, odobre@mun.ca

***Abstract*—The near-field communications have shown various improvement over the far-field ones benefiting from the unique near-field effects. However, most of the existing works exploit the benefits of near-field communications by employing a large number of antennas, which entails exorbitant hardware costs. In this paper, we consider multiuser communications based on sparse arrays (SAs) to exploit the near-field effects for sum-rate improvement with low hardware costs. To maximize the ergodic sum-rate of near-field multiuser communications, we optimize the antenna positions of SAs under the limitations of antenna panel size and antenna spacings. Using the maximum ratio combining, the maximization of the ergodic sum-rate is formulated as the minimization of the correlations among channel steering vectors. Since the problem of channel steering vector correlation minimization is nonconvex, an effective successive convex approximation-based antenna position optimization algorithm is proposed. Simulation results show that the proposed method can significantly improve the sum-rate over the existing methods with the same hardware costs.**

***Index Terms*—Antenna position optimization, near-field multiuser communications, sparse arrays, successive convex approximation**

I. Introduction

The next-generation wireless communications are expected to improve user experience and support compelling applications [1]–[3]. These anticipated developments entail heightened demands on the future communications, such as enhanced transmission rates and improved network connectivity. To meet these demands, various technologies have been developed. Among them, near-field communications have attracted widespread attention for the potential to improve the communication capacity and support various applications [3].

Generally, the radiation fields of wireless signals are categorized into the near field and the far field [4]–[9]. The Rayleigh distance, which increases quadratically with the antenna aperture and inversely with the carrier wavelength, serves as a common boundary to separate these two fields. During propagation, the electromagnetic (EM) waves exhibit a planar wavefront in the far field but a spherical wavefront in the near field. By exploiting the unique propagation characteristics in the near-field, various improvement can be achieved compared to far-field communications, such as increased channel degrees of freedom (DoF) in single-user communications [1], improved spatial resolution in multiuser communications [3], enhanced physical-layer security [4], and advanced spatial localization capabilities [5].

Most of the existing works exploit the benefits of near-field communications by employing a large number of antennas, which entails exorbitant hardware costs [4]–[6]. In fact, the implementation of the near-field communications relies on the near-field effects, which are essentially caused by large array apertures instead of large numbers of antennas. In light of this, we expand the array aperture to implement the near-field communications by increasing the spacings between adjacent antennas, which coincides with the concept of the sparse arrays (SAs). In this way, the benefits of near-field communications can be exploited with low hardware costs.

In this paper, we consider multiuser communications based on SAs to exploit the near-field effects for sum-rate improvement with low hardware costs. To maximize the ergodic sum-rate of near-field multiuser communications, we optimize the antenna positions of SAs under the limitations of antenna panel size and antenna spacings. Using the maximum ratio combining, the maximization of the ergodic sum-rate is formulated as the minimization of the correlations among channel steering vectors. To solve the nonconvex correlation minimization problem, an effective successive convex approximation-based antenna position optimization (SCA-APO) algorithm is proposed.

Notations: Symbols for matrices (upper case) and vectors (lower case) are in boldface. $(\cdot)^{\mathrm{H}}$ denotes the conjugate transpose (Hermitian). $[\boldsymbol{a}]_n$ represents the nth entry of vector $\boldsymbol{a}$, $[\boldsymbol{A}]_{:,n}$ denotes the nth column of matrix $\boldsymbol{A}$, and $[\boldsymbol{A}]_{m,n}$ refers to the entry on the mth row and nth column of matrix $\boldsymbol{A}$. Additionally, j is the square root of -1, $|\cdot|$ is the absolute value of a scalar, $\mathbb{E}\{\cdot\}$ denotes the expectation operation, and $\mathbb{C}$ is the set of complex numbers.

II. System Model

We consider the uplink transmission between K single-antenna users and a base station (BS). The BS employs an antenna panel with a length of D to accommodate an N-element sparse linear array, where we assume N is an odd number and $N \triangleq 2M+1$. To fully exploit the spatial DoF of near-field communications, the fully digital structure is adopted at the BS, which implies that each antenna is

connected to a radio frequency (RF) chain. For the SAs, due to the much larger antenna spacing than the conventional half-wavelength-interval uniform linear array (HULA), the number of antennas can be much smaller for a fixed antenna panel. Therefore, the budget of RF chains for SAs with fully digital structure can be affordable. Then, the received signals from the kth user, for $k = 1, 2, \cdots, K$, can be expressed as

$$\boldsymbol{y}_k = \boldsymbol{h}_k z_k + \eta, \tag{1}$$

where $\boldsymbol{h}_k \in \mathbb{C}^N$ represents the channel between the kth user and the BS, and z_k denotes the transmit signal of the kth user. η denotes the additive white Gaussian noise and follows $\eta \sim \mathcal{CN}(0, \sigma^2)$. We establish a Cartesian coordinate system to characterize the channels, where the tangent direction, normal direction, and center of the antenna panel are designated as the x-axis, the y-axis, and the origin, respectively. Naturally, the left and right boundaries of the antenna panel are $-D/2$ and $D/2$, respectively. Denote the coordinate of the nth antenna, for $n = -M, \cdots, 0, \cdots, M$, as $(x_n, 0)$. Typically, antenna positions are restricted to the boundaries of the antenna panel, i.e., $x_n \in [-D/2, D/2]$. To intuitively show the sparsity of the SAs, we define $p \triangleq \frac{2D}{(N-1)\lambda}$, which denotes the ratio of the length of the antenna panel to the array aperture of the N-element HULA.

According to the uniform spherical-wave model [10], the channel between the kth user and the BS can be expressed as

$$\boldsymbol{h}_k = \sum_{l=1}^{L_k} \gamma_k^{(l)} \boldsymbol{\alpha}\left(\boldsymbol{x}, r_k^{(l)}, \theta_k^{(l)}\right), \tag{2}$$

where L_k and $\boldsymbol{x} \triangleq [x_{-M}, \cdots, x_0, \cdots, x_M]^{\mathrm{T}}$ denote the number of paths between the kth user and the BS, and the stack of the antenna positions, respectively. $\gamma_k^{(l)}$, $r_k^{(l)}$, and $\theta_k^{(l)}$ denote the channel gain, channel distance, and channel physical angle-of-departure (AoD) of the lth path between the kth user and the BS, respectively. $\boldsymbol{\alpha}\left(\boldsymbol{x}, r_k^{(l)}, \theta_k^{(l)}\right)$, which is a function of $\boldsymbol{x}$, $r_k^{(l)}$ and $\theta_k^{(l)}$, denotes the channel steering vector for the lth path between the kth user and the BS. We omit the superscript and subscript in $r_k^{(l)}$ and $\theta_k^{(l)}$ for simplicity, and express $\boldsymbol{\alpha}(\boldsymbol{x}, r, \theta)$ as

$$\left[\boldsymbol{\alpha}(\boldsymbol{x}, r, \theta)\right]_n = e^{j2\pi\left(\widetilde{r}^{(n)} - r\right)/\lambda}, \tag{3}$$

for $n = -M, \cdots, 0, \cdots, M$, where λ denotes the carrier wavelength. $\widetilde{r}^{(n)}$ represents the distance between the nth antenna of the SA and the user and can be expressed as

$$\widetilde{r}^{(n)} = \sqrt{r^2 - 2rx_n \sin\theta + x_n^2}. \tag{4}$$

The complex expression in (4) poses great difficulties to the system implementation and performance analysis. To simplify the expression, we approximate $\widetilde{r}^{(n)}$ by

$$\widetilde{r}^{(n)} \approx r - x_n \sin\theta + \frac{x_n^2(1 - \sin^2\theta)}{2r} \tag{5}$$

according to $\sqrt{1+\epsilon} \approx 1 + \epsilon/2 - \epsilon^2/8$, which is verified to be accurate in the radiative near field, i.e., $r \geq 0.62\sqrt{D^3/\lambda}$ [10]. Define $\Theta \triangleq \sin\theta$ and

$$b \triangleq \frac{(1 - \Theta^2)}{2r}. \tag{6}$$

Since the physical AoD usually satisfies $\theta \in [-\pi/2, \pi/2]$, we have $\Theta \in [-1, 1]$. When r tends to infinity, b achieves its minimum value of zero. When Θ equals zero and r equals the minimum distance of the BS coverage, b achieves its maximum value of $b_{\max}$. Therefore, we have $b \in [0, b_{\max}]$. Substituting (5) and (6) into (3), the channel steering vector can be simplified as

$$[\boldsymbol{\alpha}(\boldsymbol{x}, r, \theta)]_n \approx e^{j2\pi\left(bx_n^2 - \Theta x_n\right)/\lambda}. \tag{7}$$

From (7), the simplified channel steering vector is a function of $\boldsymbol{x}$, b, and Θ. We denote the simplified channel steering vector as $\boldsymbol{\gamma}(\boldsymbol{x}, b, \Theta)$, i.e.,

$$[\boldsymbol{\gamma}(\boldsymbol{x}, b, \Theta)]_n = e^{j2\pi\left(bx_n^2 - \Theta x_n\right)/\lambda}. \tag{8}$$

III. Antenna Position Optimization of Sparse Arrays

In this section, we optimize the antenna positions of the SAs to maximize the ergodic sum-rate of near-field multiuser communications, where an SCA-APO algorithm is proposed.

The multiuser sum-rate can be expressed as

$$R_{\mathrm{sum}} = \sum_{k=1}^{K} \log_2(1 + \Gamma_k). \tag{9}$$

Γ_k denotes the signal-to-interference-plus-noise ratio of the kth user and can be expressed as

$$\Gamma_k = \frac{|\boldsymbol{h}_k^{\mathrm{H}} \boldsymbol{f}_k|^2}{\sum_{i=1, i\neq k}^{K} |\boldsymbol{h}_k^{\mathrm{H}} \boldsymbol{f}_i|^2 + \sigma^2}, \tag{10}$$

where $\boldsymbol{f}_k$ denotes the beamformer for the kth user. Note that the antenna positions are typically fixed after installation. Therefore, we optimize the antenna positions by considering the ergodic sum-rate. Then the antenna position optimization problem can be formulated as

$$\text{(P1)} \quad \max_{\boldsymbol{x}} \ \mathbb{E}\{R_{\mathrm{sum}}\} \tag{11a}$$

$$\text{s.t.} \quad |x_n - x_m| \geq \lambda/2 \tag{11b}$$

$$x_n \geq -D/2, \ x_n \leq D/2 \tag{11c}$$

$$m, n = -M, \cdots, 0, \cdots M, \ m \neq n,$$

where the objective in (11a) aims at maximizing the expectation of sum-rate with respect to $\boldsymbol{h}_k$, the constraint in (11b) denotes the minimum antenna spacing limitation to avoid the coupling effects between adjacent antennas, and the constraint in (11c) denotes the space limitation of the antenna panel. In fact, solving the problem in (11) is difficult due to three challenges: 1) Calculating the expectation of sum-rate with respect to $\boldsymbol{h}_k$ is challenging due to the highly nonlinear relationships. 2) The minimum antenna spacing constraint in (11b) is not convex. 3) The objective in (11a) is a nonconvex function of the antenna positions. Subsequently, we will focus on these three challenges and find solutions for (11).

A. For the First Challenge: Simplification of (11a)

According to Jensen's inequality, we have

$$\mathbb{E}\{R_{\mathrm{sum}}\} \geq \sum_{k=1}^{K} \log_2\left(1 + \left(\mathbb{E}\{\Gamma_k^{-1}\}\right)^{-1}\right). \tag{12}$$

To streamline our analysis, we opt to optimize the lower bound of $\mathbb{E}\{R_{\mathrm{sum}}\}$, i.e., $\sum_{k=1}^{K} \log_2(1 + \mathbb{E}\{\Gamma_k^{-1}\}^{-1})$. In

addition, since the expectation transverses all possibilities of the channels, $\mathbb{E}\{\Gamma_k^{-1}\}$ would be the same for all the users. Therefore, we can focus on the analysis of an arbitrary user and convert (11) to

$$\text{(P2)} \qquad \min_{\boldsymbol{x}} \quad \mathbb{E}\{\Gamma_k^{-1}\} \tag{13a}$$

$$\text{s.t.} \quad \text{(11b) and (11c).} \tag{13b}$$

To further simplify (13), we adopt the maximum ratio combining, which is widely employed for multiuser capacity analysis due to its ability in assessing multiuser interference (MUI) [11]. By setting $\boldsymbol{f}_k = \boldsymbol{h}_k/\boldsymbol{h}_k^{\mathrm{H}}\boldsymbol{h}_k$, for $k = 1, 2, \cdots, K$, the denominator of $\mathbb{E}\{\Gamma_k^{-1}\}$ will be a constant. Thus, the minimization of $\mathbb{E}\{\Gamma_k^{-1}\}$ in (13a) can be converted to the minimization of the numerator of $\mathbb{E}\{\Gamma_k^{-1}\}$, i.e., $\mathbb{E}\{\sum_{i=1,i\neq k}^{K}|\boldsymbol{h}_k^{\mathrm{H}}\boldsymbol{h}_i|^2/|\boldsymbol{h}_i^{\mathrm{H}}\boldsymbol{h}_i|^2+\sigma^2\}$. Note that

$$\begin{aligned}
&\mathbb{E}\left\{\sum_{i=1,i\neq k}^{K}\left|\boldsymbol{h}_k^{\mathrm{H}}\boldsymbol{h}_i\right|^2/\left|\boldsymbol{h}_i^{\mathrm{H}}\boldsymbol{h}_i\right|^2+\sigma^2\right\}\\
&\overset{(a)}{=}\mathbb{E}\left\{\sum_{i=1,i\neq k}^{K}\left|\boldsymbol{h}_k^{\mathrm{H}}\boldsymbol{h}_i\right|^2/\left|\boldsymbol{h}_i^{\mathrm{H}}\boldsymbol{h}_i\right|^2\right\}+\sigma^2\\
&\overset{(b)}{=}(K-1)\mathbb{E}\left\{\left|\boldsymbol{h}_k^{\mathrm{H}}\boldsymbol{h}_i\right|^2/\left|\boldsymbol{h}_i^{\mathrm{H}}\boldsymbol{h}_i\right|^2\right\}+\sigma^2,
\end{aligned} \tag{14}$$

where (a) holds because σ^2 is a constant and (b) holds because the expectation of MUI is the same for all users. Then, the objective in (13) can be converted to the minimization of

$$\begin{aligned}
&\mathbb{E}\left\{\left|\boldsymbol{h}_k^{\mathrm{H}}\boldsymbol{h}_i\right|^2/\left|\boldsymbol{h}_i^{\mathrm{H}}\boldsymbol{h}_i\right|^2\right\}\\
&\overset{(a)}{=}\sum_{l=1}^{L_k}\sum_{u=1}^{L_i}\mathbb{E}\left\{\frac{\left|\gamma_k^{(l)}\gamma_i^{(u)}\right|^2}{\left|\boldsymbol{h}_i^{\mathrm{H}}\boldsymbol{h}_i\right|^2}\left|\boldsymbol{\alpha}\left(\boldsymbol{x},r_k^{(l)},\theta_k^{(l)}\right)^{\mathrm{H}}\boldsymbol{\alpha}\left(\boldsymbol{x},r_i^{(u)},\theta_i^{(u)}\right)\right|^2\right\}\\
&\overset{(b)}{=}\sum_{l=1}^{L_k}\sum_{u=1}^{L_i}\xi_k^{(l)}\widetilde{\xi}_i^{(u)}\mathbb{E}\left\{\left|\boldsymbol{\alpha}\left(\boldsymbol{x},r_k^{(l)},\theta_k^{(l)}\right)^{\mathrm{H}}\boldsymbol{\alpha}\left(\boldsymbol{x},r_i^{(u)},\theta_i^{(u)}\right)\right|^2\right\},
\end{aligned} \tag{15}$$

where (a) holds because $\mathbb{E}\{\gamma_k^{(l)}\}=0$, and we define $\xi_k^{(l)} \triangleq \mathbb{E}\{|\gamma_k^{(l)}|^2\}$ and $\widetilde{\xi}_i^{(u)} \triangleq \mathbb{E}\{|\gamma_i^{(u)}|^2/|\boldsymbol{h}_i^{\mathrm{H}}\boldsymbol{h}_i|^2\}$ in (b). Due to the expectation operation, the minimization of (15) can be converted to the minimization of

$$\begin{aligned}
&\mathbb{E}\left\{\left|\boldsymbol{\alpha}\left(\boldsymbol{x},r_k^{(l)},\theta_k^{(l)}\right)^{\mathrm{H}}\boldsymbol{\alpha}\left(\boldsymbol{x},r_i^{(u)},\theta_i^{(u)}\right)\right|^2\right\}\\
&\overset{(a)}{\approx}\mathbb{E}\left\{\left|\boldsymbol{\gamma}\left(\boldsymbol{x},b_k^{(l)},\Theta_k^{(l)}\right)^{\mathrm{H}}\boldsymbol{\gamma}\left(\boldsymbol{x},b_i^{(u)},\Theta_i^{(u)}\right)\right|^2\right\}\\
&=\mathbb{E}\left\{\left|\sum_{n=-M}^{M}e^{j2\pi\left(\left(b_i^{(u)}-b_k^{(l)}\right)x_n^2+\left(\Theta_k^{(l)}-\Theta_i^{(u)}\right)x_n\right)/\lambda}\right|^2\right\}\\
&\overset{(b)}{=}\mathbb{E}\left\{\left|\sum_{n=-M}^{M}e^{j2\pi\left(\overline{\overline{b}}x_n^2+\overline{\overline{\Theta}}x_n\right)/\lambda}\right|^2\right\},
\end{aligned} \tag{16}$$

where (a) holds by adopting the approximation in (8), and we define $\overline{\overline{b}} \triangleq b_i^{(u)} - b_k^{(l)}$ and $\overline{\overline{\Theta}} \triangleq \Theta_k^{(l)} - \Theta_i^{(u)}$ in (b). Note that (16) essentially denotes the correlations among channel steering vectors.

One remaining problem is how to calculate the expectation in (16). Obtaining the closed-form solution of the expectation in (16) is challenging due to the highly nonlinear relationships. Therefore, we turn to calculating (16) via numerical methods. Note that $b_i^{(u)}, b_k^{(l)} \in [0, b_{\max}]$ and $\Theta_k^{(l)}, \Theta_i^{(u)} \in [-1, 1]$. Therefore, we have $\overline{\overline{b}} \in [-b_{\max}, b_{\max}]$ and $\overline{\overline{\Theta}} \in [-2, 2]$. We quantize the intervals of $\overline{\overline{b}}$ and $\overline{\overline{\Theta}}$ into S and T samples, respectively, where the sth sample of $\overline{\overline{b}}$ and tth sample of $\overline{\overline{\Theta}}$ can be expressed as

$$\begin{aligned}
\widehat{b}_s &= -b_{\max} + \frac{2(s-1)b_{\max}}{S},\\
\widehat{\Theta}_t &= -2 + \frac{4(t-1)}{T}.
\end{aligned} \tag{17}$$

Then, we calculate the distribution of different samples. Without loss of generality, we assume $b_i^{(u)}$ and $b_k^{(l)}$ follow the uniform distribution within $[0, b_{\max}]$ while $\Theta_k^{(l)}$ and $\Theta_i^{(u)}$ follow the uniform distribution within $[-1, 1]$. The probability distribution functions of $\overline{\overline{b}}$ and $\overline{\overline{\Theta}}$ can be further expressed as

$$f\left(\overline{\overline{b}}\right) = \frac{1}{b_{\max}} - \frac{1}{b_{\max}^2}\left|\overline{\overline{b}}\right|, \text{ for } \overline{\overline{b}} \in [-b_{\max}, b_{\max}], \tag{18}$$

and

$$g\left(\overline{\overline{\Theta}}\right) = \frac{1}{2} - \frac{1}{4}\left|\overline{\overline{\Theta}}\right|, \text{ for } \overline{\overline{\Theta}} \in [-2, 2]. \tag{19}$$

With (17), (18) and (19), the expectation in (16) can be expressed as

$$\begin{aligned}
&\mathbb{E}\left\{\left|\sum_{n=-M}^{M}e^{j2\pi\left(\overline{\overline{b}}x_n^2+\overline{\overline{\Theta}}x_n\right)/\lambda}\right|^2\right\}\\
&\approx\frac{1}{ST}\sum_{s=1}^{S}\sum_{t=1}^{T}w_{t,s}\left|\sum_{n=-M}^{M}e^{j2\pi\left(\widehat{b}_s x_n^2+\widehat{\Theta}_t x_n\right)/\lambda}\right|^2\\
&\triangleq h(\boldsymbol{x}),
\end{aligned} \tag{20}$$

where $w_{t,s} \triangleq f\left(\widehat{b}_s\right)g\left(\widehat{\Theta}_t\right)$.

B. For the Second Challenge: Conversion of (11b)

Now, we turn to solving the nonconvex constraint in (11b). This constraint is designed to regulate the separation between adjacent antennas. In the context of linear arrays, the antennas are arranged in a line. We can ensure adherence to the minimum spacing constraint by maintaining a specified distance between the current antenna and the former one. Consequently, the constraint in (11b) can be converted to

$$x_n - x_{n-1} > \lambda/2, \text{ for } n = -M+1, \cdots, 0, \cdots, M, \tag{21}$$

which is a convex constraint.

C. For the Third Challenge: SCA-APO Algorithm

Based on (20) and (21), (P2) can be converted to

$$\text{(P3)} \qquad \min_{\boldsymbol{x}} \quad h(\boldsymbol{x}) \tag{22a}$$

$$\text{s.t.} \quad \text{(21) and (11c).} \tag{22b}$$

Note that (P3) is an optimization problem with nonconvex objective and convex constraints. To deal with the nonconvex objective in (22a), we then propose a successive convex approximation-based antenna position optimization (SCA-APO) algorithm.

Algorithm 1 Successive Convex Approximation-based Antenna Position Optimization (SCA-APO) Algorithm

Input: D, Q and N.
Initialization: $q \leftarrow 0$. Generate $\boldsymbol{x}^{(0)}$ randomly.
while $q < Q$ **do**
  $q \leftarrow q + 1$.
  Obtain $\boldsymbol{x}^{(q)}$ by solving (P3-q).
end while
$\widehat{\boldsymbol{x}} \leftarrow \boldsymbol{x}^{(Q)}$.
Output: $\widehat{\boldsymbol{x}}$.

First of all, we randomly initialize the antenna positions as $\boldsymbol{x}^{(0)}$.

In the qth iteration, for $q \geq 1$, the key point of the SCA is to find a convex surrogate function that can locally approximate the original function around $\boldsymbol{x}^{(q-1)}$ and is also the upper bound of the original function. According to the Taylor's theorem [12], we have

$$\begin{aligned} h(\boldsymbol{x}) &\leq h\big(\boldsymbol{x}^{(q-1)}\big) + \nabla h\big(\boldsymbol{x}^{(q-1)}\big)^{\mathrm{T}}\big(\boldsymbol{x} - \boldsymbol{x}^{(q-1)}\big) \\ &\quad + \frac{\chi}{2}\big(\boldsymbol{x} - \boldsymbol{x}^{(q-1)}\big)^{\mathrm{T}}\big(\boldsymbol{x} - \boldsymbol{x}^{(q-1)}\big) \\ &\triangleq \overline{h}\big(\boldsymbol{x}, \boldsymbol{x}^{(q-1)}\big), \end{aligned} \tag{23}$$

where $\nabla h\big(\boldsymbol{x}^{(q-1)}\big)$ denotes the gradient vector and χ denotes the maximum eigenvalue of the Hessian matrix $\nabla^2 h\big(\boldsymbol{x}^{(q-1)}\big)$. The gradient vector $\nabla h\big(\boldsymbol{x}\big)$ and the Hessian matrix $\nabla^2 h\big(\boldsymbol{x}\big)$ are provided in (24) and (25), respectively, which are shown at the top of the next page.

Then, the qth subproblem can be expressed as

$$\text{(P3-}q\text{)} \qquad \min_{\boldsymbol{x}} \ \overline{h}\big(\boldsymbol{x}, \boldsymbol{x}^{(q-1)}\big) \tag{26a}$$

$$\text{s.t.} \ \ (21) \text{ and } (11c). \tag{26b}$$

Obviously, (P3-q) is a convex problem and therefore can be effectively solved. We omit the details and denote the solution of (P3-q) as $\boldsymbol{x}^{(q)}$.

We iteratively solve (P3-q) until the maximum number of iterations Q is reached, where we denote the optimized antenna position as $\widehat{\boldsymbol{x}}$. Finally, we summarize the SCA-APO algorithm in **Algorithm 1**.

Now we analyze the convergence of the SCA-APO algorithm. Note that

$$h(\boldsymbol{x}^{(q)}) \overset{\text{(a)}}{\leq} \overline{h}(\boldsymbol{x}^{(q)}, \boldsymbol{x}^{(q-1)}) \overset{\text{(b)}}{\leq} \overline{h}(\boldsymbol{x}^{(q-1)}, \boldsymbol{x}^{(q-1)}) \overset{\text{(c)}}{=} h(\boldsymbol{x}^{(q-1)}) \tag{27}$$

where we obtain (a) according to (23), obtain (b) because $\boldsymbol{x}^{(q)}$ is the optimal solution of (26), and obtain (c) by comparing the expressions of $\overline{h}\big(\boldsymbol{x}^{(q-1)}, \boldsymbol{x}^{(q-1)}\big)$ and $h\big(\boldsymbol{x}^{(q-1)}\big)$ in (23). According to (27), we have $h\big(\boldsymbol{x}^{(q)}\big) \leq h\big(\boldsymbol{x}^{(q-1)}\big)$, which indicates that the objective value will decrease with the iteration and therefore the SCA-APO algorithm converges.

We also analyze the computational complexity of the SCA-APO algorithm. The SCA-APO algorithm contains Q iterations. In each iteration, the computational complexity mainly comes from solving (26). In fact, (26) is a typical convex quadratic programming problem and its computational complexity is $\mathcal{O}(N^{3.5})$. In total, the computational complexity of the proposed SCA-APO algorithm is $\mathcal{O}(QN^{3.5})$.

IV. Simulation Results

Now, we evaluate the performance of the considered near-field multiuser communications based on SAs. The BS employs an SA with 33 antennas to serve K users. The communication systems operate at the carrier frequency of 30 GHz, which corresponds to the carrier wavelength of 0.01 m. The channel between the BS and the kth user contains one line-of-sight path and two non-line-of-sight paths, where the Ricean K-factor is denoted as κ. For the SCA-APO algorithm, we set the maximum number of iterations as $Q = 100$. We also perform the multiuser communications with the uniform circular array (UCA) in [13] and the conventional HULA, which are adopted as benchmarks. The widely-spaced uniform array (WSUA), which arrange the antennas uniformly within the antenna panel, is also adopted as the benchmark. For a fair comparison, the UCA, HULA and WSUA have the same simulation configurations as the proposed SAs.

In Fig. 1, we compare the sum-rate of multiuser communications for different kinds of arrays, considering different SNRs. Specifically, we set $\kappa = -20$ dB, $K = 28$, and $p = 10$. The channel angles distribute randomly within $[-\sqrt{3}/2, \sqrt{3}/2]$, while the channel distances distribute randomly within $[10, 100]$ m. From the figure, when the SNR is low, e.g., less than -10 dB, the four arrays achieve similar performance. In fact, this similarity arises from the substantial deterioration caused by the noise, which impacts the effectiveness of each array. However, at high SNRs, the four arrays have different performance. Specifically, the sum-rate of the UCA is notably lower than those of the other three arrays. This is because the adoption of a circular array configuration for a fixed number of antennas results in a significantly reduced array aperture compared to the other three arrangements. This reduced array aperture, in turn, adversely affects angle resolution and exacerbates the MUI. In contrast, the proposed SA demonstrates significantly higher sum-rate than the UCA and HULA, which can be attributed to the larger array apertures of the SAs. The expanded array aperture of the SA enables the exploitation of near-field effects, which increases the spatial resolution and consequently increases the sum-rate of multiuser communications. Notably, despite similar array apertures, the proposed SA outperforms the WSUA. This superior performance benefits from the proposed SA's ability to mitigate the grating lobes, thereby reducing MUI and increasing the sum-rate.

In Fig. 2, we compare the sum-rate of multiuser communications for different kinds of arrays, considering different numbers of users. We fix the SNR as 20 dB. The array sparsity factor, the distribution of the channel angles and the distribution of the channel distances are the same as those in Fig. 1. When the number of users is small, e.g., $K \leq 5$, all the four arrays can provide enough spatial DoF to separate multiple users. As a result, the four arrays have similar performance in terms of sum-rate. With the increase of K, the sum-rate of the four arrays all initially

$$\left[\nabla h(\boldsymbol{x})\right]_n = \sum_{s=1}^{S}\sum_{t=1}^{T}\frac{4\pi w_{t,s}(2\widehat{b}_s x_n + \widehat{\Theta}_t)}{ST\lambda}\sum_{v=-M}^{M}\sin\left(\frac{2\pi}{\lambda}\left(\widehat{b}_s(x_v^2 - x_n^2) + \widehat{\Theta}_t(x_v - x_n)\right)\right). \tag{24}$$

$$\left[\nabla^2 h(\boldsymbol{x})\right]_{m,n} = \begin{cases} \sum_{s=1}^{S}\sum_{t=1}^{T}\frac{8\pi^2 w_{t,s}(2\widehat{b}_s x_n+\widehat{\Theta}_t)(2\widehat{b}_s x_m+\widehat{\Theta}_t)}{ST\lambda^2}\cos\left(\frac{2\pi}{\lambda}\left(\widehat{b}_s(x_m^2 - x_n^2) + \widehat{\Theta}_t(x_m - x_n)\right)\right), & m \neq n, \\ \sum_{s=1}^{S}\sum_{t=1}^{T}\frac{8\pi w_{t,s}\widehat{b}_s}{ST\lambda}\sum_{v=-M}^{M}\sin\left(\frac{2\pi}{\lambda}\left(\widehat{b}_s(x_v^2 - x_n^2) + \widehat{\Theta}_t(x_v - x_n)\right)\right), & m = n. \end{cases} \tag{25}$$

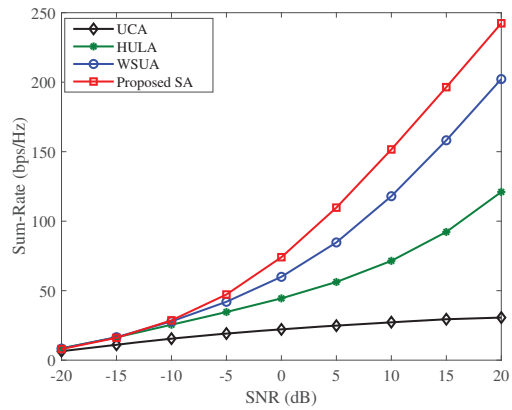

Fig. 1. Comparisons of different arrays in terms of sum-rate for different SNRs.

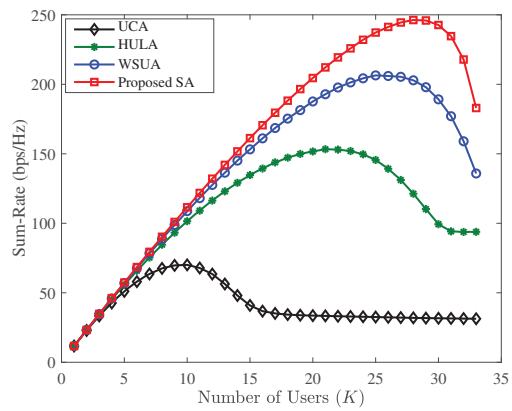

Fig. 2. Comparisons of different arrays in terms of sum-rate for different numbers of users.

increase and then decrease. This trend is attributed to the detrimental impact of strong MUI on the performance of multiuser communications when dealing with a larger number of users. Notably, the four arrays achieve the maximum sum-rate at different user numbers. Specifically, the UCA, HULA, WSUA and proposed SA achieve their peak sum-rate when the number of users equals 10, 21, 25 and 28, respectively. This observation indicates that the SAs have the potential to serve more users than the other three arrays.

V. Conclusion

In this paper, we have considered multiuser communications based on SAs to exploit the near-field effects for sum-rate improvement with low hardware costs. An effective SCA-APO algorithm has been proposed to optimize the antenna positions of SAs under the limitations of antenna panel size and antenna spacings. Simulation results have shown that the proposed method can significantly improve the sum-rate of the existing methods with the same hardware costs. In the future, we will continue our work by further exploring the potential of SAs in near-field communications.

VI. Acknowledgment

This work was supported in part by the National Natural Science Foundation of China under Grants U22B2007 and 62071116, in part by the National Key Research and Development Program of China under Grant 2021YFB2900404, and in part by the Natural Sciences and Engineering Research Council of Canada (NSERC) through its Discovery program.

References

[1] J. An, C. Yuen, L. Dai, M. D. Renzo, M. Debbah, and L. Hanzo, "Near-field communications: Research advances, potential, and challenges," *IEEE Wireless Commun.*, vol. 31, no. 3, pp. 100–107, June 2024.

[2] C. Qi, J. Wang, L. Lyu, L. Tan, J. Zhang, and G. Y. Li, "Key issues in wireless transmission for NTN-assisted Internet of Things," *IEEE Internet of Things Mag.*, vol. 7, no. 1, pp. 40–46, Jan. 2024.

[3] H. Zhang, N. Shlezinger, F. Guidi, D. Dardari, and Y. C. Eldar, "6G wireless communications: From far-field beam steering to near-field beam focusing," *IEEE Commun. Mag.*, vol. 61, no. 4, pp. 72–77, Apr. 2023.

[4] Y. Zhang, H. Zhang, S. Xiao, W. Tang, and Y. C. Eldar, "Near-field wideband secure communications: An analog beamfocusing approach," *IEEE Trans. Signal Process.*, vol. 72, pp. 2173–2187, Apr. 2024.

[5] K. Chen, C. Qi, C.-X. Wang, and G. Y. Li, "Beam training and tracking for extremely large-scale MIMO communications," *IEEE Trans. Wireless Commun.*, vol. 23, no. 5, pp. 5048–5062, May 2023.

[6] G. Bacci, L. Sanguinetti, and E. Björnson, "Spherical wavefronts improve MU-MIMO spectral efficiency when using electrically large arrays," *IEEE Wireless Commun. Lett.*, vol. 12, no. 7, pp. 1219–1223, Apr. 2023.

[7] G. Jiang and C. Qi, "Near-field beam training based on deep learning for extremely large-scale MIMO," *IEEE Commun. Lett.*, vol. 27, no. 8, pp. 2063–2067, Aug. 2023.

[8] K. Chen, C. Qi, O. A. Dobre, and G. Y. Li, "Triple-refined hybrid-field beam training for mmWave extremely large-scale MIMO," *IEEE Trans. Wireless Commun., early access*, pp. 1–15, 2024.

[9] X. Shi, J. Wang, Z. Sun, and J. Song, "Spatial-chirp codebook-based hierarchical beam training for extremely large-scale massive MIMO," *IEEE Trans. Wireless Commun.*, vol. 23, no. 4, pp. 2824–2838, Apr. 2024.

[10] M. Cui and L. Dai, "Channel estimation for extremely large-scale MIMO: Far-field or near-field?" *IEEE Trans. Commun.*, vol. 70, no. 4, pp. 2663–2677, Jan. 2022.

[11] H. Lu and Y. Zeng, "Near-field modeling and performance analysis for multi-user extremely large-scale MIMO communication," *IEEE Commun. Lett.*, vol. 26, no. 2, pp. 277–281, Feb. 2022.

[12] J. R. Magnus and H. Neudecker, *Matrix Differential Calculus With Applications in Statistics and Econometrics*. Hoboken, NJ, USA: Wiley, 1995.

[13] Z. Wu, M. Cui, and L. Dai, "Enabling more users to benefit from near-field communications: From linear to circular array," *IEEE Trans. Wireless Commun.*, vol. 23, no. 4, pp. 3735–3748, Apr. 2024.